

Sampling Network Guided Cross-Entropy Method for Unsupervised Point Cloud Registration

Haobo Jiang , Yaqi Shen , Jin Xie* , Jun Li , Jianjun Qian* , and Jian Yang

PCA Lab, Nanjing University of Science and Technology, China

{jiang.hao.bo, syq, csjxie, junli, csjqian, csjyang}@njjust.edu.cn

Abstract

In this paper, by modeling the point cloud registration task as a Markov decision process, we propose an end-to-end deep model embedded with the cross-entropy method (CEM) for unsupervised 3D registration. Our model consists of a sampling network module and a differentiable CEM module. In our sampling network module, given a pair of point clouds, the sampling network learns a prior sampling distribution over the transformation space. The learned sampling distribution can be used as a “good” initialization of the differentiable CEM module. In our differentiable CEM module, we first propose a maximum consensus criterion based alignment metric as the reward function for the point cloud registration task. Based on the reward function, for each state, we then construct a fused score function to evaluate the sampled transformations, where we weight the current and future rewards of the transformations. Particularly, the future rewards of the sampled transforms are obtained by performing the iterative closest point (ICP) algorithm on the transformed state. By selecting the top-k transformations with the highest scores, we iteratively update the sampling distribution. Furthermore, in order to make the CEM differentiable, we use the sparse-max function to replace the hard top-k selection. Finally, we formulate a Geman-McClure estimator based loss to train our end-to-end registration model. Extensive experimental results demonstrate the good registration performance of our method on benchmark datasets. Code is available at <https://github.com/Jiang-HB/CEMNet>.

1. Introduction

Point cloud registration is the problem of finding the optimal rigid transformation (i.e., a rotation matrix and a translation vector) that can align the source point cloud to the target precisely. It plays important roles in a variety of 3D vision applications such as 3D reconstruction [1, 38, 20], Lidar SLAM [12, 57], 3D object location [14, 46, 31]. However, various challenges such as outliers and noise interference still hinder its application in the real world.

Owing to discriminative feature extraction of deep neural networks, deep point cloud registration methods [48, 49, 28] have shown impressive performance. Nevertheless, most of their success mainly depends on large amounts of ground-truth transformations for supervised point cloud registration, which greatly increases their training costs. To avoid it, recent efforts have been devoted to developing an unsupervised registration model. For example, cycle consistency is used as the self-supervision signal to train the registration models in [19, 54]. However, the cycle-consistency loss may not be able to deal with the partially-overlapping case well, since the outliers cannot form a closed loop. In addition, unsupervised point cloud registration methods [47, 25] learn the transformation by minimizing the alignment error (e.g., Chamfer metric) between the transformed source point cloud and the target point cloud. Nevertheless, for a pair of point clouds with complex geometry, the optimization of the alignment error between them may be difficult and prone to sticking into the local minima.

Inspired by the model based reinforcement learning (RL) [22, 21], in this paper, we propose a novel sampling network guided cross-entropy method for unsupervised point cloud registration. By formulating the 3D registration task as a Markov decision process (MDP), it is expected to heuristically search for the optimal transformation by gradually narrowing its interest transformation region through trial and error. Our deep unsupervised registration model consists of two modules, i.e., sampling network module and differentiable cross-entropy method (CEM) module. Given a

*Corresponding authors

Haobo Jiang, Yaqi Shen, Jin Xie, Jun Li, Jianjun Qian and Jian Yang are with PCA Lab, Key Lab of Intelligent Perception and Systems for High-Dimensional Information of Ministry of Education, and Jiangsu Key Lab of Image and Video Understanding for Social Security, School of Computer Science and Engineering, Nanjing University of Science and Technology, China.

pair of source and target point clouds, the sampling network aims to learn a prior Gaussian distribution over the transformation space, which can provide the subsequent CEM module a proper initialization. With the learned sampling distribution, the differentiable CEM further searches for the optimal transformation by iteratively sampling the transformation candidates, evaluating the candidates, and updating the distribution. Specifically, in the sampling network module, we utilize the learned matching map with the local geometric feature for the mean estimation of the sampling distribution and exploit the global feature for variance estimation, respectively. In the CEM module, a novel fused score function combining the current and the future rewards is designed to evaluate each sampled transformation. Particularly, the future reward is estimated by performing the ICP algorithm on the transformed source point cloud and the target point cloud. In addition, the differentiability in our CEM module is achieved by softening the sorting based top- k selection with a differentiable sparsemax function. Finally, we formulate a scaled Geman-McClure estimator [58] based loss function to train our model, where the sublinear convergence speed for the outliers can weaken the negative impact on registration precision from the outliers.

To summarize, our main contributions are as follows:

- We propose a novel end-to-end cross-entropy method based deep model for unsupervised point cloud registration, where a prior sampling distribution is predicted by a sampling network to quickly focus on the promising searching region.
- In the cross-entropy method, we design a novel ICP driven fused reward function for accurate transformation candidate evaluation and propose a sparsemax function based soft top- k selection mechanism for the differentiability of our model.
- Compared to the unsupervised or even some fully supervised deep methods, our method can obtain outstanding performance on extensive benchmarks.

2. Related Work

Traditional point cloud registration algorithms. In the traditional 3D registration field, a lot of research has focused on the Iterative Closest Point algorithm (ICP) [6] and its variants. The original ICP repeatedly performs correspondence estimation and transformation optimization to find the optimal transformation. However, ICP with improper initialization easily sticks into the local minima dilemma and the sensitivity to the outliers also degrades its performance in the partially overlapping case. To avoid it, Go-ICP [53] globally searches for the optimal transformation via integrating the branch-and-bound scheme into the ICP. Furthermore, Chetverikov *et al.* [7] proposed a trimmed ICP (TrICP) algorithm to handle the partial case,

where the least square optimization is only performed on partial minimum square errors rather than the all. Moreover, other variants such as [40, 16, 4, 18, 11] also present competitive registration performance. In addition, RANSAC based methods [15, 10, 9, 45, 44, 13] also have been extensively studies. Among them, one representative method is the 4PCS [2, 42, 43] which determines the correspondence from the sampled four-point sets that are nearly co-planar via comparing their intersectional diagonal ratios. Furthermore, Super4PCS [33], an improved 4PCS method, is proposed to largely reduce the computational complexity of the congruent four-point sets sampling. Compared with the quadratic time complexity of points in 4PCS, Super4PCS only requires linear complexity, which greatly promotes its application in the real world. In addition, other RANSAC variants, including [35, 34, 52, 24, 17, 27] also show good alignment results.

Learning-based point cloud registration algorithms. In recent years, deep learning based point cloud registration methods have received widespread attention. PPFNet method [11] is proposed to utilize the PointNet [37] to extract the feature of the point patches and then perform the RANSAC for finding corresponding patches. DCP [48] calculates the rigid transformation via the singular value decomposition (SVD) where the correspondence is constructed through learning a soft matching map. RPM-Net [55] also realizes the registration based on the matching map generated from the Sinkhorn layer and annealing. [56] aligns the point cloud pair by minimizing the KL-Divergence between two learned Gaussian Mixture Models. In addition, ReAgent [5] is proposed to combine the imitation learning and model-free reinforcement learning (i.e., proximal policy optimization [39]) for registration agent training. Instead, our method utilizes the model-based cross-entropy method for registration with the constructed MDP model. [26] proposes to search for the optimal solution by planning with a learned latent dynamic model. Although it's unsupervised and has a faster inference speed, the approximation error in its latent reward and translation networks may potentially degrade its registration precision. Moreover, [19, 54] propose to apply the cycle consistency as the supervision signal into the point cloud registration for the unsupervised learning. However, since the non-overlapping region cannot construct a closed-loop, they also may not handle the partial case well. In addition, other learning-based methods, including [49, 28, 8, 36, 30, 29, 59] also present impressive performance.

3. Approach

3.1. Problem Setting

For the point cloud registration task, given the source point cloud $\mathbf{X} = \{\mathbf{x}_i \in \mathbb{R}^3 \mid i = 1, \dots, N\}$ and the target

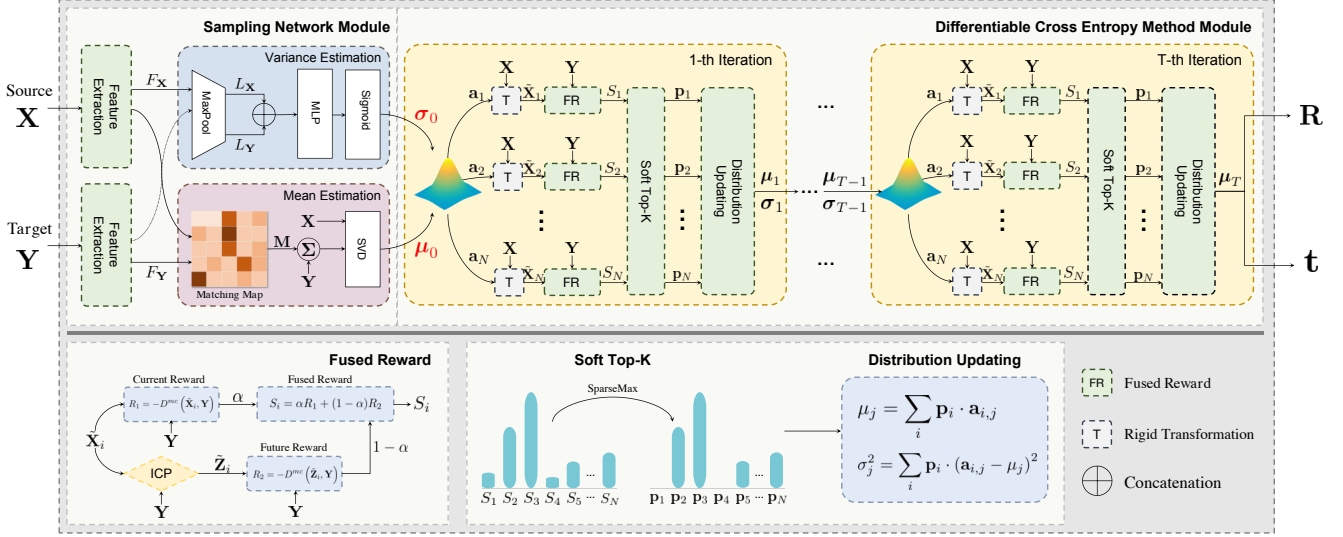


Figure 1. The pipeline of the proposed sampling network guided cross-entropy method (CEM) for point cloud registration. Our framework mainly contains two cascaded modules: (a) Sampling network module: Given the source and target point clouds $\{\mathbf{X}, \mathbf{Y}\}$, we extract their per-point features F_X and the global feature L_Y which are used to predict the mean μ_0 and the standard deviation σ_0 of the initial sampling distribution ($\mathcal{N}(\mu_0, \sigma)$) for subsequent CEM block. (b) Differentiable CEM module: In the t -th iteration ($1 \leq t \leq T$), it alternatively performs the sampling transformation candidates $\{\mathbf{a}_1, \dots, \mathbf{a}_N\}$; evaluating sampled transformations (obtaining scores $\{S_1, \dots, S_N\}$) through our designed fused score function which combines the current and future rewards; mapping the obtained scores to a sparse distribution $\{\mathbf{p}_1, \dots, \mathbf{p}_N\}$ with the differentiable sparsemax function; updating the sampling distribution via Eq. 8. In the last iteration, we use the expected value of the sampling distribution to estimate the optimal transformation.

point cloud $\mathbf{Y} = \{\mathbf{y}_j \in \mathbb{R}^3 \mid j = 1, \dots, M\}$, we aim to recover the rigid transformation containing a rotation matrix $\mathbf{R} \in SO(3)$ and a translation vector $\mathbf{t} \in \mathbb{R}^3$ for aligning the two point clouds. In this work, we formulate 3D point cloud registration as a Markov decision process (MDP), which contains a state set, an action set, a state transition function, and a reward function.

State space. We define the set of point cloud pairs as the state space \mathcal{S} , that is $\mathbf{s} = \{\mathbf{X}, \mathbf{Y}\} \in \mathcal{S}$.

Action space. We denote the rigid transformation space $SE(3)$ ($SO(3) \times \mathbb{R}^3$) as the action space \mathcal{A} . To reduce the dimension of the search space, we utilize the Euler angle representation $\mathbf{e} = [e_1, e_2, e_3] \in [-\pi, \pi]^3$ to encode the rotation $\mathbf{R} \in SO(3)$. Thus, the action $\mathbf{a} \in \mathcal{A}$ is represented by $\mathbf{a} = [\mathbf{e}, \mathbf{t}]$ and $\mathbf{R}(\mathbf{e})$ is denoted as the corresponding rotation matrix of the Euler angle \mathbf{e} .

State transition function. After executing the action $\mathbf{a} = [\mathbf{e}, \mathbf{t}]$ at the current state $\mathbf{s} = \{\mathbf{X}, \mathbf{Y}\}$, we predict the next registration state $\mathbf{s}' = \{\tilde{\mathbf{X}}, \mathbf{Y}\}$ with the state transition function \mathcal{T} , that is:

$$\mathbf{s}' = \mathcal{T}(\mathbf{s}, \mathbf{a}) = \left\{ \{\mathbf{R}(\mathbf{e}) \mathbf{x}_i + \mathbf{t}\}_{i=1}^N, \mathbf{Y} \right\} = \{\tilde{\mathbf{X}}, \mathbf{Y}\}. \quad (1)$$

Reward function. We evaluate the effect of executing the action \mathbf{a} at the state \mathbf{s} with the reward function $R(\mathbf{s}, \mathbf{a})$ in the point cloud registration task. In order to handle the partially overlapping case, we define a maximum consensus criterion based alignment metric D^{mc} as below to quan-

tify the reward, that is, $R(\mathbf{s}, \mathbf{a}) = -D^{mc}(\mathcal{T}(\mathbf{s}, \mathbf{a})) = -D^{mc}(\tilde{\mathbf{X}}, \mathbf{Y})$. The lower the alignment error between $\tilde{\mathbf{X}}$ and \mathbf{Y} , the higher the reward obtained by that action:

$$D^{mc}(\tilde{\mathbf{X}}, \mathbf{Y}) = 2 - \frac{1}{N} \sum_{\tilde{\mathbf{x}}_i \in \tilde{\mathbf{X}}} \rho_\varepsilon(d_{\tilde{\mathbf{x}}_i, \mathbf{Y}}) \left(1 - \frac{d_{\tilde{\mathbf{x}}_i, \mathbf{Y}}}{\varepsilon} \right) - \frac{1}{M} \sum_{\mathbf{y}_j \in \mathbf{Y}} \rho_\varepsilon(d_{\mathbf{y}_j, \tilde{\mathbf{X}}}) \left(1 - \frac{d_{\mathbf{y}_j, \tilde{\mathbf{X}}}}{\varepsilon} \right), \quad (2)$$

where $d_{\tilde{\mathbf{x}}_i, \mathbf{Y}} = \min_{\mathbf{y}_j} \|\tilde{\mathbf{x}}_i - \mathbf{y}_j\|_2$ denotes the shorest distance between the point $\tilde{\mathbf{x}}_i$ and the point cloud \mathbf{Y} and $\rho_\varepsilon(x) = 1 \{x \leq \varepsilon\}$ is the indicator function, where the threshold $\varepsilon > 0$ is a hyper-parameter that specifies the maximum allowable distance for inlier. D^{mc} measures the alignment error via counting the number of overlapping point pairs, which can effectively relieve the effect of outliers. Furthermore, each count in D^{mc} is weighted with $1 - d_{\tilde{\mathbf{x}}_i, \mathbf{Y}}/\varepsilon$. Compared to the discrete count [27], such weighting operation enforces the overlapping pair to be as close as possible rather than just no more than the maximum allowable distance.

Lemma 1 *If the threshold ε is no less than the maximum of distances between all closest point pairs, that is, $\max \{ \max_i d_{\tilde{\mathbf{x}}_i, \mathbf{Y}}, \max_j d_{\mathbf{y}_j, \tilde{\mathbf{X}}} \} \leq \varepsilon < \infty$, D^{mc} is proportional to the Chamfer metric D^{cd} with ratio $1/\varepsilon$, i.e.,*

$$D^{mc}(\tilde{\mathbf{X}}, \mathbf{Y}) = 1/\varepsilon \cdot D^{cd}(\tilde{\mathbf{X}}, \mathbf{Y}).$$

The proof is provided in Appendix A.

Based on the constructed MDP, given a source and target point cloud pair $\mathbf{s} = \{\mathbf{X}, \mathbf{Y}\}$, the point cloud registration task aims to find the optimal action \mathbf{a}^* by maximizing its reward as below:

$$\mathbf{a}^* = \underset{\mathbf{a} \in \mathcal{A}}{\operatorname{argmax}} R(\mathbf{s}, \mathbf{a}) = \underset{\mathbf{a} \in \mathcal{A}}{\operatorname{argmin}} D^{mc}(\mathcal{T}(\mathbf{s}, \mathbf{a})). \quad (3)$$

3.2. Differentiable Cross-Entropy Method based Deep Registration Network

To solve the optimization problem in Eq. 3, we propose a novel CEM based unsupervised cloud registration framework. As shown in Fig. 1, our deep model contains two cascaded modules, including a sampling network module and a differentiable CEM module. With the source and target point cloud pair as the input, the sampling network module predicts a sampling distribution over the transformation space (Section 3.2.1). Guided by this sampling distribution, the CEM module searches the optimal transformation by iteratively narrowing the search space through the transformation sampling, transformation evaluation, and distribution updating. The optimal transformation can be estimated with the mean of the elite transformations in the last iteration (Section 3.2.2).

3.2.1 Sampling Network Module

Given the source and target point cloud pair $\mathbf{s} = \{\mathbf{X}, \mathbf{Y}\}$, the traditional CEM randomly samples candidates from a pre-defined sampling distribution. Instead, we aim to sample them with a learned Gaussian distribution $\{\mu_0, \sigma_0\} = \mathcal{P}(\mathbf{s}; \mathbf{w})$ parameterized by the deep neural network with parameters \mathbf{w} , so that given a registration state, it can increase the chance that sampled candidates fall into the neighborhood of the optimal transformation. As shown in Fig. 1, we utilize the Dynamic Graph CNN (DGCNN) [50] to extract the local geometric features $F_{\mathbf{X}} \in \mathbb{R}^{N \times P}$ and $F_{\mathbf{Y}} \in \mathbb{R}^{M \times P}$ via constructing the k -NN graph for each point in $\{\mathbf{X}, \mathbf{Y}\}$. With the learned point embeddings, we further generate a matching map $\mathbf{M} \in \mathbb{R}^{N \times M}$ with the softmax function:

$$\mathbf{M}_{i,j} = \operatorname{softmax}(F_{\mathbf{Y}} F_{\mathbf{x}_i}^\top)_j, \quad (4)$$

where $F_{\mathbf{x}_i} \in F_{\mathbf{X}}$ denotes the feature of the point \mathbf{x}_i and the element $\mathbf{M}_{i,j}$ denotes the matching probability of the points \mathbf{x}_i and \mathbf{y}_j . With the map \mathbf{M} , we can estimate the “matching” point $\hat{\mathbf{y}}_i$ of \mathbf{x}_i :

$$\hat{\mathbf{y}}_i = \sum_{j=1}^M \mathbf{M}_{i,j} \cdot \mathbf{y}_j \in \mathbb{R}^3. \quad (5)$$

Once the correspondences $\{(\mathbf{x}_i, \hat{\mathbf{y}}_i) \mid i = 1, \dots, N\}$ are obtained, we employ the singular value decomposition (SVD) to calculate the transformation $\{\mathbf{R}, \mathbf{t}\}$. The expected

value μ_0 of the Gaussian distribution is equal to the concatenated vector $[\mathbf{e}, \mathbf{t}] \in \mathbb{R}^6$, where \mathbf{e} is the corresponding Euler angle of \mathbf{R} . For the prediction of the standard deviation σ_0 , we first extract the global features of the point cloud pair $L_{\mathbf{X}} \in \mathbb{R}^P$ and $L_{\mathbf{Y}} \in \mathbb{R}^P$ via the maxpooling operation, that is, $L_{\mathbf{X}} = \operatorname{MaxPool}(F_{\mathbf{X}})$. Then, we feed the concatenated global feature $[L_{\mathbf{X}}, L_{\mathbf{Y}}]$ into the 3-layer MLP followed by a sigmoid function to output σ_0 .

Algorithm 1 CEM based deep registration framework

Input: state $\mathbf{s} = \{\mathbf{X}, \mathbf{Y}\}$, sampling network $\mathcal{P}(\mathbf{s}; \mathbf{w})$, iteration times T , action candidate numbers N , iteration times M of using future reward.

```

1: Initialize sampling distribution  $\{\mu_0, \sigma_0\} = p_0(\mathbf{s}; \mathbf{w})$ .
2: for  $t = 0 : T - 1$  do
3:   for  $i = 1 : N$  do
4:     Sample transformation  $\mathbf{a}_t^i \sim \mathcal{N}(\mu_t, \sigma_t^2 \mathbb{I})$ .
5:     Perform  $\mathbf{a}_t^i$  at the state  $\mathbf{s}$  and obtain the next state  $\mathbf{s}'_i$  and reward  $R(\mathbf{s}, \mathbf{a}_t^i)$ .
6:     if  $t \geq M$  then
7:       % Only-current reward.
8:       Score  $S(\mathbf{s}, \mathbf{a}_t^i) = R(\mathbf{s}, \mathbf{a}_t^i)$ .
9:     else
10:      % Fused reward.
11:      Perform ICP to registrate  $\mathbf{s}'_i$  and obtain the predicted transformation  $\mathbf{a}_{icp}^i$ .
12:      Calculate the  $R(\mathbf{s}'_i, \mathbf{a}_{icp}^i)$  as the future reward.
13:      Calculate fused score  $S(\mathbf{s}, \mathbf{a}_t^i)$  via Eq. 6.
14:     end if
15:   end for
16:   Calculate the sparsemax based weight vector via Eq. 10 and update the distribution via Eq. 8.
17: end for
Return:  $\mu_T$ 

```

3.2.2 Differentiable Cross-entropy Method Module

Guided by the prior sampling distribution learned by the network guidance module, the CEM model further iteratively searches for the optimal transformation by extensive trial and error. During the iterative process, we propose a novel fused score function combining the current reward and the ICP based future reward for accurate transformation evaluation. Furthermore, we also propose a novel differentiable CEM for the end-to-end training, where the hard top- k operation is replaced by a differentiable sparsemax function. Specifically, in the t -th iteration ($0 \leq t < T$), it executes the three steps as below:

(a) Transformation candidates sampling. In this step, we randomly sample N transformation candidates $\mathcal{C}_t = \{\mathbf{a}_t^i \mid i = 1, \dots, N\}$ from a Gaussian distribution $g_t = \mathcal{N}(\mu_t, \sigma_t^2 \mathbb{I})$. Note that we exploit the prior distribution $\{\mu_0, \sigma_0\} = \mathcal{P}(\mathbf{s}; \mathbf{w})$ predicted by the sampling network

for the first iteration so that it can quickly focus on the most promising transformation region for the optimal solution searching. For differentiability, we utilize the reparameterization trick to sample each candidate, that is, $\mathbf{a}_t^i = \boldsymbol{\mu}_t + \epsilon_i \cdot \boldsymbol{\sigma}_t$, where $\epsilon_i \sim \mathcal{N}(\mathbf{0}, \mathbb{I})$.

(b) Fused reward based transformation evaluation. After sampling the transformation candidates, based on our constructed MDP, we can obtain the corresponding rewards $\{R(\mathbf{s}, \mathbf{a}_t^i) \mid 1 \leq i \leq N\}$ for the sampled transformation candidates. In the traditional CEM, the reward is directly used to score each transformation, i.e., the score function $S(\mathbf{s}, \mathbf{a}_t^i) = R(\mathbf{s}, \mathbf{a}_t^i)$. However, a good transformation candidate needs to own not only the high current reward but also the high future reward. For example, as shown in Fig. 2, although the transformation \mathbf{a}_2 can temporarily obtain a higher reward than \mathbf{a}_1 due to the more overlapping pairs, the resulting registration state by performing \mathbf{a}_2 has a worse pose than the state by performing \mathbf{a}_1 intuitively. Thus, for a transformation, just focusing on the current reward and ignoring the future reward of a transformation may mislead the evolution of the CEM and cause it to stick into the local optima. Therefore, for each transformation, we need to define a future reward to determine whether the transformed source and target point clouds have good poses at the next registration state.

In our method, we utilize the ICP algorithm to quantify the future reward of a transformation. Specifically, we first perform each sampled transformation at the state \mathbf{s} and obtain a set of states $\{\mathbf{s}'_1, \dots, \mathbf{s}'_N\}$ where $\mathbf{s}'_i = \mathcal{T}(\mathbf{s}, \mathbf{a}_t^i) = \{\tilde{\mathbf{X}}_i, \mathbf{Y}\}$. Then, we use ICP to predict the transformation \mathbf{a}_{icp}^i for the registration state \mathbf{s}'_i , and obtain the corresponding next state $\{\tilde{\mathbf{Z}}_i, \mathbf{Y}\}$ and the reward $R(\mathbf{s}'_i, \mathbf{a}_{icp}^i) = -D^{mc}(\tilde{\mathbf{Z}}_i, \mathbf{Y})$. Finally, we use this reward as the future reward. The higher reward means \mathbf{a}_t^i may lead to a better pose at the next registration state. After that, we utilize the weighted sum of the current and future rewards to score each action:

$$S(\mathbf{s}, \mathbf{a}_t^i) = \alpha \cdot R(\mathbf{s}, \mathbf{a}_t^i) + (1 - \alpha) \cdot R(\mathbf{s}'_i, \mathbf{a}_{icp}^i), \quad (6)$$

where $\alpha \in [0, 1]$ is the hyper-parameter for balancing the weights of the current and future rewards. Note that benefiting from the CUDA programming, we accelerate the inference speed with the batch ICP consisting of the batch SVD and point-wise parallelization for closest point search.

(c) Sparsemax based distribution updating. In this step, we aim to use the elite transformations to update the sampling distribution so that more “better” candidates are expected to be sampled in the next iteration. In the traditional CEM, the top- k transformations \mathcal{I}_t with the highest scores are used as the elites to guide the distribution updat-

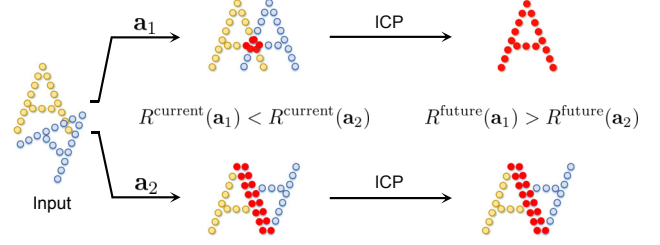


Figure 2. After performing the actions \mathbf{a}_1 and \mathbf{a}_2 on the source point cloud (blue), the transformed source point cloud via \mathbf{a}_2 has more overlapping pairs (red) with the target point cloud (yellow) than those via \mathbf{a}_1 (i.e., larger current reward, $R^{\text{current}}(\mathbf{a}_1) < R^{\text{current}}(\mathbf{a}_2)$). However, the action \mathbf{a}_1 can lead to a better pose for performing the ICP alignment. Thus, the future reward of the action \mathbf{a}_1 is higher than that of the action \mathbf{a}_2 ($R^{\text{future}}(\mathbf{a}_1) > R^{\text{future}}(\mathbf{a}_2)$).

ing $g_{t+1} = \mathcal{N}(\boldsymbol{\mu}_{t+1}, \boldsymbol{\sigma}_{t+1}^2 \mathbb{I})$ by the updating formula:

$$\boldsymbol{\mu}_{t+1,i} = \frac{1}{k} \sum_{\mathbf{a} \in \mathcal{I}_t} \mathbf{a}_i, \quad \boldsymbol{\sigma}_{t+1,i}^2 = \frac{1}{k} \sum_{\mathbf{a} \in \mathcal{I}_t} (\mathbf{a}_i - \boldsymbol{\mu}_{t+1,i})^2, \quad (7)$$

where $i = 1, \dots, 6$. In fact, Eq. 7 is the closed-form solution of the maximum likelihood estimation problem over the elites, that is, $\{\boldsymbol{\mu}_{t+1}, \boldsymbol{\sigma}_{t+1}\} = \arg\max_{\boldsymbol{\mu}, \boldsymbol{\sigma}} \sum_{\mathbf{a} \in \mathcal{I}_t} f(\mathbf{a}; \boldsymbol{\mu}, \boldsymbol{\sigma})$, where $f(\cdot; \boldsymbol{\mu}, \boldsymbol{\sigma})$ denotes the probability density function of $\mathcal{N}(\boldsymbol{\mu}, \boldsymbol{\sigma}^2)$. By re-fitting the sampling distribution with the top- k samples, the updated sampling distribution tends to focus on the more promising transformation region. However, since the sorting in the top- k operation is non-differentiable, such distribution updating method cannot be directly used for end-to-end training directly. Therefore, we propose to soften the hard top- k selection via a differentiable sparsemax function [32], which is different from LML layer used in [3]. For a clear insight, we first rewrite Eq. 7 as:

$$\boldsymbol{\mu}_{t+1,i} = \sum_{\mathbf{a} \in \mathcal{C}_t} p(\mathbf{a}) \mathbf{a}_i, \quad \boldsymbol{\sigma}_{t+1,i}^2 = \sum_{\mathbf{a} \in \mathcal{C}_t} p(\mathbf{a}) (\mathbf{a}_i - \boldsymbol{\mu}_{t+1,i})^2 \quad (8)$$

where $p(\mathbf{a}) = \frac{1}{k} \cdot \mathbb{1}\{\mathbf{a} \in \mathcal{I}_t\}$ is the weight assigned to each candidate $\mathbf{a}_t^i \in \mathcal{C}_t$ for distribution updating and the sum of all elements in $\mathbf{p} = [p(\mathbf{a}_t^1), \dots, p(\mathbf{a}_t^N)]$ is 1. Next, given the score vector $\mathbf{q} = [S(\mathbf{s}, \mathbf{a}_t^1), \dots, S(\mathbf{s}, \mathbf{a}_t^N)]$ of all candidates, sparsemax based weight vector $\tilde{\mathbf{p}}$ is defined as the solution of the following minimization problem:

$$\tilde{\mathbf{p}} = \text{sparsemax}(\mathbf{q}) = \arg\min_{\mathbf{z} \in \Delta^{N-1}} \|\mathbf{z} - \mathbf{q}\|^2, \quad (9)$$

where $\Delta^{N-1} = \{\mathbf{z} \in \mathbb{R}^N \mid \sum_i \mathbf{z}_i = 1, \mathbf{z}_i \geq 0\}$ is a $(N-1)$ -dimensional simplex. Eq. 9 has a closed-form solution, that is $\text{sparsemax}_i(\mathbf{q}) = [S(\mathbf{s}, \mathbf{a}_t^i) - \tau(\mathbf{q})]_+$, and the threshold function $\tau(\mathbf{q})$ can be expressed as:

$$\tau(\mathbf{q}) = \frac{\sum_{j \leq \mathcal{M}(\mathbf{q})} \mathbf{q}_{(j)} - 1}{\mathcal{M}(\mathbf{q})}, \quad (10)$$

where $\mathbf{q}_{(j)}$ denotes the j -largest value in the vector \mathbf{q} and $\mathcal{M}(\mathbf{q}) = \max\{m \mid 1 + m\mathbf{q}_{(m)} > \sum_{j \leq m} \mathbf{q}_{(j)}\}$ [32].

The more details about the function τ and the Jacobian of sparsemax for back propagation can be seen in Appendix B. Note that the sparsemax function maps the scores of candidates to a probability distribution whose some elements will be zero if the scores of the corresponding candidates are too low. Compared to the softmax function, the sparsemax function can adaptively ignore the negative effect of the bad candidates, which better simulates the hard top- k operation. Moreover, instead of assigning the same weight ($1/k$) to the candidates, the sparsemax function assigns the higher weights to the better candidates. Thus, the updated distribution can focus on the actions with the higher scores and more potential candidates in the next iteration can be sampled. After T iterations, we use the expected value of the sampling distribution to estimate the optimal transformation. The CEM based registration algorithm is outlined in Algorithm 1.

3.3. Loss Function

Under the unsupervised setting, we utilize the alignment error between the transformed source point cloud and target point cloud rather than the ground-truth transformation for model training. To handle the partially-overlapping case well, a proper robust loss function insensitive to the outliers is desired. In this paper, we integrate the scaled Geman-McClure estimator ρ_μ [58] into our loss function:

$$\rho_\mu(x) = \frac{\mu \cdot x^2}{\mu + x^2}, \quad (11)$$

where the Geman-McClure estimator has the sublinear convergent speed for the outliers and thus can weaken their negative impact on the registration precision. The hyper-parameter μ determines the range of the inliers. Given a training dataset $\mathcal{D} = \{(\mathbf{X}_i, \mathbf{Y}_i)\}$, the loss function $\mathcal{L}(\mathbf{w})$ is defined as below:

$$\mathcal{L}(\mathbf{w}) = \mathbb{E}_{\mathbf{X}, \mathbf{Y} \sim \mathcal{D}} \left[\frac{1}{|\mathbf{X}|} \sum_{\tilde{\mathbf{x}}_i \in \tilde{\mathbf{X}}(\mathbf{w})} \rho_\mu(d_{\tilde{\mathbf{x}}_i, \mathbf{Y}}) + \frac{1}{|\mathbf{Y}|} \sum_{\mathbf{y}_i \in \mathbf{Y}} \rho_\mu(d_{\mathbf{y}_i, \tilde{\mathbf{X}}(\mathbf{w})}) \right], \quad (12)$$

where $\tilde{\mathbf{X}}(\mathbf{w})$ denotes the transformed source point cloud after performing the transformation predicted by our deep model on the source point cloud \mathbf{X} .

4. Experiment

In this section, we perform extensive experiments and ablation studies on benchmark datasets, including the *ModelNet40* [51], *7Scene* [41] and *ICL-NUIM* [23]. We simply name our CEM based Registration Network as **CEMNet**.

4.1. Implementation Details

We train our model using Adam optimizer with learning rate 10^{-4} , and weight decay 5×10^{-4} for 50 epochs.

The batch size is set to 32. In our differentiable CEM module, we set the numbers of iterations T and candidates N to 15 and 1000, respectively, and the maximum allowable distance ε is set to 0.1. For the fused reward for transformation evaluation, we set M to 3 and the impact weight α in the score function is set to 0.5. The hyper-parameter μ in the Geman-McClure estimator used in our loss function is set to 0.01. We utilize PyTorch to implement our project and perform all experiments on the server equipped with a 2080Ti GPU and an Intel i5 2.2GHz CPU.

4.2. Evaluation on ModelNet40

We first test our method on the *ModelNet40* dataset [51], which contains 40 categories and is constructed via uniformly sampling 1,024 points from each of 12,311 CAD models. Then, we divide it into two parts where 2,468 models are used for testing and the remaining models are for training. Following the setting in [48], we first generate a random rotation matrix and translation vector via uniformly sampling in the Euler angle range $[0, 45^\circ]$ and the translation range $[-0.5, 0.5]$. Then, we use the transformed source point cloud as the target point cloud and the generated transformation is as the ground truth. The metric for evaluating the registration precision contains the *root mean squared error (RMSE)* and *mean absolute error (MAE)* between the predicted transformation and the ground-truth transformation, where the error about Euler angle uses the degree as the unit. We compare our method with eight state-of-the-art methods, where ICP [6], Go-ICP [53], Super4PCS [33], SDRSAC [27] and FGR [58] belong to the traditional methods, and IDAM [28] and DCP-v2 [48] are fully supervised deep methods while FMR [25] is unsupervised. Some visualization results are presented in Fig. 3 and more qualitative examples can be seen in Appendix D.

Partially overlapping unseen object. We first evaluate our method on partially overlapping unseen objects, where the test and training datasets contain all 40 categories, and the non-overlapping region may still exist in the perfectly aligned point clouds. Following [49], to construct the partially overlapping point clouds, we first randomly sample a point in source and target point clouds, respectively. Then, we perform the farthest point subsampling (FPS) to sample 75% (768) points while the remaining 25% points are viewed as the missing points and discarded. We utilize the implementations provided by the authors to train FMR, DCP-v2, and IDAM on our modified training dataset with partial overlap. The left column of Table 1 shows that compared to other algorithms, our unsupervised method can obtain superior registration performance with all evaluation metrics and even exceeds the fully supervised DCP-v2 and IDAM, which owes to that the CEM module guided by the sampling network can effectively search for the accurate transformation.

Partially overlapping unseen category. To further test the

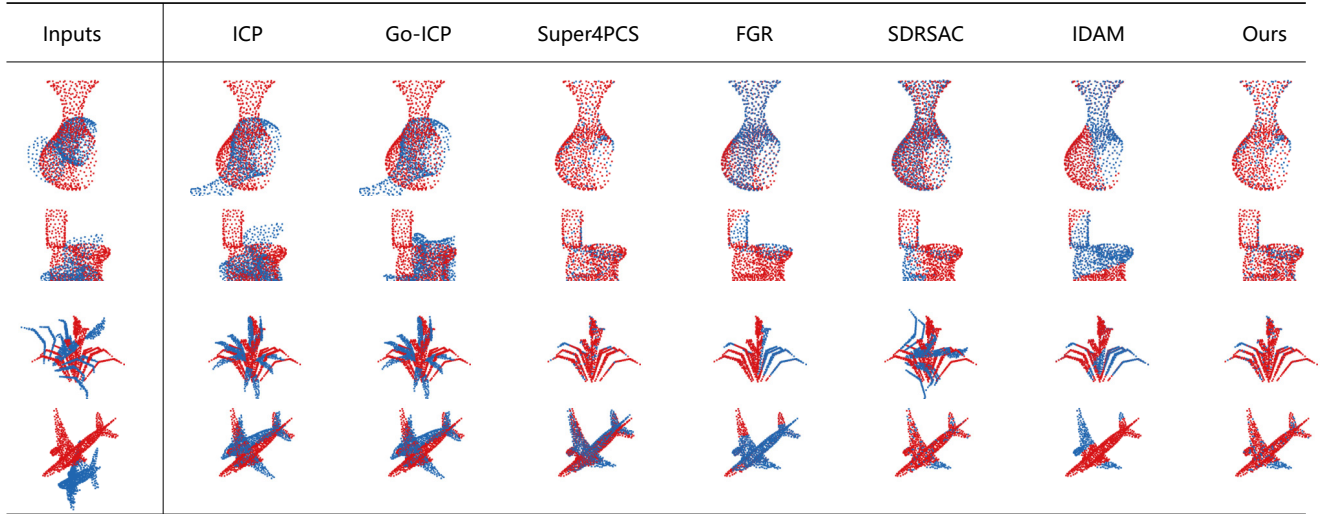


Figure 3. Qualitative registration examples on partially overlapping *ModelNet40* dataset.

Model	Unseen object				Unseen category				Unseen object with noise			
	RMSE(R)	RMSE(t)	MAE(R)	MAE(t)	RMSE(R)	RMSE(t)	MAE(R)	MAE(t)	RMSE(R)	RMSE(t)	MAE(R)	MAE(t)
ICP [6] (*)	13.7952	0.0391	4.4483	0.0196	14.7732	0.0351	3.5938	0.0132	12.5413	0.0398	4.2826	0.0184
Go-ICP [53] (*)	14.7223	0.0328	3.5112	0.0127	13.8322	0.0321	3.1579	0.0121	14.5225	0.0329	3.4252	0.0114
Super4PCS [33] (*)	<u>1.5764</u>	<u>0.0034</u>	5.3512	0.0214	2.5186	<u>0.0032</u>	1.4364	0.0041	12.4551	0.0201	1.3780	0.0033
SDRSAC [27] (*)	3.9173	0.0121	2.7956	0.0102	4.2475	0.0139	3.0144	0.0121	<u>0.4719</u>	<u>0.0185</u>	2.3965	0.0164
FGR [58] (*)	3.7055	0.0088	0.5972	<u>0.0020</u>	3.1251	0.0074	<u>0.4469</u>	<u>0.0013</u>	0.4712	0.0703	0.2353	0.0404
DCP-v2 [48] (◇)	4.8962	0.0248	3.3297	0.0169	6.3787	0.0246	4.4222	0.0173	5.1575	0.0251	3.4708	0.0176
IDAM [28] (◇)	2.3384	0.0102	<u>0.4711</u>	0.0025	<u>2.1566</u>	0.0151	0.6135	0.0037	3.5701	0.0206	1.0642	<u>0.0066</u>
FMR [25] (△)	9.0997	0.0204	3.6497	0.0101	9.1322	0.0223	3.8593	0.0113	5.5605	0.0194	2.5437	0.0072
CEMNet (ours, △)	1.5018	0.0009	0.1385	0.0001	1.1013	0.0020	0.0804	0.0002	2.2722	0.0014	<u>0.3799</u>	0.0008

Table 1. Comparison results on partially overlapping *ModelNet40* dataset. (*), (△) and (◇) denote the traditional, unsupervised and fully supervised deep methods, respectively.

Dataset	Model	RMSE(R)	RMSE(t)	MAE(R)	MAE(t)
7Scene	ICP [6] (*)	19.9166	0.1127	7.5760	0.0310
	Go-ICP [53] (*)	24.2743	0.0360	7.1068	0.0137
	Super4PCS [33] (*)	19.2603	0.3646	15.7001	0.2898
	SDRSAC [27] (*)	0.3501	0.4997	0.2925	0.4997
	FGR [58] (*)	<u>0.2724</u>	0.0011	<u>0.1380</u>	<u>0.0006</u>
	DCP-v2 [48] (◇)	7.5548	0.0411	5.6991	0.0303
	IDAM [28] (◇)	10.5306	0.0539	5.6727	0.0303
	FMR [25] (△)	8.6999	0.0199	3.6569	0.0101
	CEMNet (ours, △)	0.1768	<u>0.0012</u>	0.0434	0.0002
ICL-NUIM	ICP [6] (*)	10.1247	0.3006	2.1484	0.0693
	Go-ICP [53] (*)	<u>1.5514</u>	0.0601	<u>0.6333</u>	0.0241
	Super4PCS [33] (*)	28.8616	0.3091	24.1373	0.2502
	SDRSAC [27] (*)	9.4074	0.2477	7.8627	0.2076
	FGR [58] (*)	3.0423	0.1275	1.9571	0.0659
	DCP-v2 [48] (◇)	9.2142	<u>0.0191</u>	6.5826	<u>0.0134</u>
	IDAM [28] (◇)	9.4539	0.3040	4.4153	0.1385
	FMR [25] (△)	1.8282	0.0685	1.1085	0.0398
	CEMNet (ours, △)	0.0821	0.0002	0.0211	0.0001

Table 2. Comparison results on *7Scene* and *ICL-NUIM* datasets. (*), (△) and (◇) denote the traditional, unsupervised and fully supervised deep methods, respectively.

generalization ability of our model, we utilize 20 categories for training and then test the trained model on another 20 unseen categories. The comparison results are listed in the middle column of Table 1. Our method presents good gen-

eralization ability on unseen categories and still obtains the best scores on all criteria.

Partially overlapping unseen object with noise. For the robustness evaluation of our method in the presence of noise, we jitter each point of the partially overlapping source and target point clouds with Gaussian noise. Following [49], we sample the noise in each axis, clipped by $[-0.05, 0.05]$, from a Gaussian distribution with the mean 0 and the standard deviation 0.01. The right column of Table 1 demonstrates that although it is worse than FGR in terms of the *RMSE* and *MAE* criteria with respect to rotation, it yields better performance on translation.

4.3. Evaluation on 7Scene and ICL-NUIM

We further evaluate our method on two indoor datasets: *7Scene* and *ICL-NUIM*. The former consists of seven scenes: Chess, Fires, Heads, Office, Pumpkin, Redkitchen, and Stairs, and is split into two parts, one containing 296 scans for training and the other containing 57 scans as the test dataset. The latter is split into 1, 278 and 200 scans for training and test, respectively. As in Sec. 4.2, we exploit the FPS operation to obtain the partial point clouds

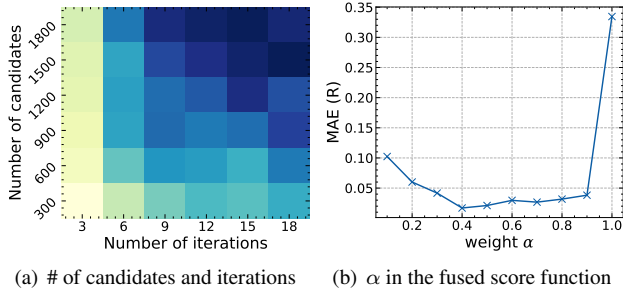


Figure 4. Rotation errors in the cases of (a) different numbers of candidates and iterations, and (b) different weights in fused score function on *ICL-NUIM* dataset.

SN	Future	dCEM	<i>ModelNet40^{uc}</i>		<i>ICL-NUIM</i>	
			MAE(R)	MAE(t)	MAE(R)	MAE(t)
✓			4.4222	0.0173	6.5826	0.0134
		✓	1.8625	0.0041	1.8333	0.0023
	✓	✓	0.3675	<u>0.0004</u>	0.8364	0.0048
✓		✓	<u>0.1781</u>	<u>0.0004</u>	<u>0.3345</u>	<u>0.0005</u>
✓	✓	✓	0.0804	0.0002	0.0211	0.0001

Table 3. Ablation study of different components on *ModelNet40^{uc}* (unseen category) and *ICL-NUIM* datasets. *SN*: Sampling network module; *Future*: ICP driven future reward evaluation; *dCEM*: differentiable CEM module.

and use the transformed source point cloud as the target point cloud, where the transformation is also generated via randomly sampling. As demonstrated in Table 2, on *ICL-NUIM*, our method exhibits higher registration precision on all criteria. In addition, on *7Scene*, our method is slightly worse than FGR in terms of the *RMSE* of translation but shows the lower alignment errors on other criteria.

4.4. Ablation Study and Analysis

Sampling network module. As shown in the fourth and fifth rows of Table 3, equipped with the sampling network module (*SN*), *dCEM* (differentiable CEM) and *dCEM+Future* (differentiable CEM with future reward) can obtain significant error reduction on all criteria. This is because that *SN* can learn a better initial sampling distribution, which assists the *dCEM* to efficiently search for the optimal solution. Note that we use the Gaussian distribution $\mathcal{N}(\mathbf{0}, \mathbf{1}\mathbf{I})$ as the pre-defined sampling distribution for our method without *SN*. Moreover, since the sampling network has a similar model design as DCP-v2 except for the branch used for variance prediction, the results in the first row refer to the scores of the fully supervised DCP-v2. One can see that without planning in the CEM module, *SN* yields poor performance, even guided by the ground truth transformation, which implies the necessity of the proposed CEM module for the precise registration.

Fused score function. We further evaluate the effect of ICP based future reward in the fused score function of CEM. As shown in the second and fourth rows of Table 3, the perfor-

# Future (<i>M</i>)	Time (ms)	<i>ModelNet40^{uc}</i>		<i>ModelNet40^{uo}</i>	
		MAR(R)	MAR(t)	MAE(R)	MAE(t)
0	184.7	0.1782	0.00040	0.3505	0.00053
1	<u>235.5</u>	0.1709	0.00021	0.2688	0.00018
2	263.7	0.1198	0.00019	0.2137	0.00015
3	309.5	<u>0.0804</u>	<u>0.00015</u>	<u>0.1385</u>	<u>0.00012</u>
4	335.2	0.0470	0.00011	0.1258	0.00010

Table 4. The time and precision vary with different number of iterations using ICP driven potential evaluation on *ModelNet40^{uc}* (unseen category) and *ModelNet40^{uo}* (unseen object) datasets.

mance drops significantly without considering the future reward of the transformation candidate. Furthermore, Table 4 also shows that as the iteration times *M* of using the future reward increases, the error keeps decreasing while the time cost continues to increase. To balance the performance and speed, we set *M* to 3 in all experiments. Finally, we test the fluctuation of the error with different weights α in the fused function. Fig. 4(b) shows that a good balance between the current and future rewards tends to bring higher precision.

Parameters in CEM. We test the sensitivity of the hyperparameters in CEM, including the numbers of the iterations *T* and the candidates *N*. Fig. 4(a) shows that as *T* and *N* increase, the error tends to decrease (from the light color to the dark color). However, as shown in Appendix C, their performance gain is at the cost of the inference time and we set *N* and *T* to 1000 and 10 in all experiments.

Inference time. We use the averaged running time on each case from *ModelNet40* dataset (unseen object) to evaluate the inference time of each algorithm. Note that the traditional registration methods are performed on Intel i5 2.2GHz CPU while the deep learning based methods are executed on 2080Ti GPU. The time cost of our method is 310ms, while the cost of the other methods are ICP (14ms), Go-ICP (2, 278ms), Super4PCS (6, 790ms), FGR (75ms), SDRSAC (23, 651ms), FMR (414ms), DCP-v2 (34ms), and IDAM (53ms), respectively.

5. Conclusion

In this paper, we proposed a novel sampling network guided cross-entropy method for unsupervised point cloud registration. In our framework, the sampling network is used to provide a prior sampling distribution for CEM. Guided by this learnable distribution, the CEM module further heuristically searches for the optimal transformation. During this optimization process, we designed a fused score function combining current and ICP based future rewards for more accurate transformation evaluation. Furthermore, we also replaced the hard top-*k* selection with the differentiable sparsemax function for the end-to-end model training.

Acknowledgments

This work was supported by the National Science Fund of China (Grant Nos. U1713208, 61876084, 61876083, 62072242).

References

- [1] Sameer Agarwal, Yasutaka Furukawa, Noah Snavely, Ian Simon, Brian Curless, Steven M Seitz, and Richard Szeliski. Building rome in a day. *Communications of the ACM* (2011), 54(10):105–112.
- [2] Dror Aiger, Niloy J Mitra, and Daniel Cohen-Or. 4-points congruent sets for robust pairwise surface registration. In *SIGGRAPH* (2008).
- [3] Brandon Amos and Denis Yarats. The differentiable cross-entropy method. In *ICML* (2020).
- [4] Kwang-Ho Bae and Derek D Lichti. A method for automated registration of unorganised point clouds. *Journal of Photogrammetry and Remote Sensing* (2008), 63(1):36–54.
- [5] Dominik Bauer, Timothy Patten, and Markus Vincze. ReAgent: Point cloud registration using imitation and reinforcement learning. In *CVPR* (2021).
- [6] Paul J Besl and Neil D McKay. Method for registration of 3-D shapes. In *Sensor fusion IV: control paradigms and data structures* (1992), volume 1611, pages 586–606.
- [7] Dmitry Chetverikov, Dmitry Svirko, Dmitry Stepanov, and Pavel Krsek. The trimmed iterative closest point algorithm. In *Object recognition supported by user interaction for service robots* (2002), volume 3, pages 545–548.
- [8] Christopher Choy, Wei Dong, and Vladlen Koltun. Deep global registration. In *CVPR* (2020), pages 2514–2523.
- [9] Ondrej Chum and Jiri Matas. Matching with PROSAC-progressive sample consensus. In *CVPR* (2005).
- [10] Ondřej Chum, Jiří Matas, and Josef Kittler. Locally optimized RANSAC. In *Joint Pattern Recognition Symposium* (2003), pages 236–243.
- [11] Haowen Deng, Tolga Birdal, and Slobodan Ilic. PPFNet: Global context aware local features for robust 3D point matching. In *CVPR* (2018).
- [12] Jean-Emmanuel Deschaud. IMLS-SLAM: Scan-to-model matching based on 3D data. In *ICRA* (2018).
- [13] Zhen Dong, Fuxun Liang, Bisheng Yang, Yusheng Xu, Yufu Zang, Jianping Li, Yuan Wang, Wenxia Dai, Hongchao Fan, Juha Hyypä, et al. Registration of large-scale terrestrial laser scanner point clouds: A review and benchmark. *Journal of Photogrammetry and Remote Sensing* (2020), 163:327–342.
- [14] Bertram Drost, Markus Ulrich, Nassir Navab, and Slobodan Ilic. Model globally, match locally: Efficient and robust 3D object recognition. In *CVPR* (2010).
- [15] Martin A Fischler and Robert C Bolles. Random sample consensus: a paradigm for model fitting with applications to image analysis and automated cartography. *Communications of the ACM* (1981), 24(6):381–395.
- [16] Andrew W Fitzgibbon. Robust registration of 2D and 3D point sets. *Image and vision computing* (2003), 21(13-14):1145–1153.
- [17] Xuming Ge. Automatic markerless registration of point clouds with semantic-keypoint-based 4-points congruent sets. *ISPRS Journal of Photogrammetry and Remote Sensing* (2017), 130:344–357.
- [18] Adrien Gressin, Clément Mallet, Jérôme Demantké, and Nicolas David. Towards 3D lidar point cloud registration improvement using optimal neighborhood knowledge. *ISPRS journal of photogrammetry and remote sensing* (2013), 79:240–251.
- [19] Thibault Groueix, Matthew Fisher, Vladimir G Kim, Bryan C Russell, and Mathieu Aubry. Unsupervised cycle-consistent deformation for shape matching. In *Computer Graphics Forum* (2019), volume 38, pages 123–133.
- [20] Changjun Gu, Yang Cong, and Gan Sun. Three birds, one stone: Unified laser-based 3-D reconstruction across different media. *TIM* (2021).
- [21] Danijar Hafner, Timothy Lillicrap, Jimmy Ba, and Mohammad Norouzi. Dream to control: Learning behaviors by latent imagination. *arXiv preprint arXiv:1912.01603* (2019).
- [22] Danijar Hafner, Timothy Lillicrap, Ian Fischer, Ruben Villegas, David Ha, Honglak Lee, and James Davidson. Learning latent dynamics for planning from pixels. In *ICML* (2019).
- [23] Ankur Handa, Thomas Whelan, John McDonald, and Andrew J Davison. A benchmark for RGB-D visual odometry, 3D reconstruction and SLAM. In *ICRA* (2014).
- [24] Jida Huang, Tsz-Ho Kwok, and Chi Zhou. V4PCS: Volumetric 4PCS algorithm for global registration. *Journal of Mechanical Design* (2017), 139(11).
- [25] Xiaoshui Huang, Guofeng Mei, and Jian Zhang. Feature-metric registration: A fast semi-supervised approach for robust point cloud registration without correspondences. In *CVPR* (2020).
- [26] Haobo Jiang, Jianjun Qian, Jin Xie, and Jian Yang. Planning with learned dynamic model for unsupervised point cloud registration. *IJCAI* (2021).
- [27] Huu M Le, Thanh-Toan Do, Tuan Hoang, and Ngai-Man Cheung. SDRSAC: Semidefinite-based randomized approach for robust point cloud registration without correspondences. In *CVPR* (2019).
- [28] Jiahao Li, Changhao Zhang, Ziyao Xu, Hangning Zhou, and Chi Zhang. Iterative distance-aware similarity matrix convolution with mutual-supervised point elimination for efficient point cloud registration. In *ECCV* (2020).
- [29] Xiang Li, Lingjing Wang, and Yi Fang. PC-Net: Unsupervised point correspondence learning with neural networks. In *3DV* (2019).
- [30] Xiang Li, Lingjing Wang, and Yi Fang. Unsupervised partial point set registration via joint shape completion and registration. *arXiv preprint arXiv:2009.05290* (2020).
- [31] Yuyang Liu, Yang Cong, Gan Sun, Zhang Tao, Jiahua Dong, and Hongsen Liu. L3DOC: Lifelong 3D object classification. *TIP* (2021).
- [32] Andre Martins and Ramon Astudillo. From softmax to sparsemax: A sparse model of attention and multi-label classification. In *ICML* (2016).
- [33] Nicolas Mellado, Dror Aiger, and Niloy J Mitra. Super 4pcs fast global pointcloud registration via smart indexing. In *Computer graphics forum* (2014), volume 33, pages 205–215.
- [34] Mustafa Mohamad, Mirza Tahir Ahmed, David Rappaport, and Michael Greenspan. Super generalized 4pcs for 3D registration. In *3DV* (2015).

- [35] Mustafa Mohamad, David Rappaport, and Michael Greenspan. Generalized 4-points congruent sets for 3D registration. In *3DV (2014)*, volume 1, pages 83–90.
- [36] G Dias Pais, Srikumar Ramalingam, Venu Madhav Govindu, Jacinto C Nascimento, Rama Chellappa, and Pedro Miraldo. 3DRegNet: A deep neural network for 3D point registration. In *CVPR (2020)*.
- [37] Charles R Qi, Hao Su, Kaichun Mo, and Leonidas J Guibas. PointNet: Deep learning on point sets for 3D classification and segmentation. In *CVPR (2017)*, pages 652–660.
- [38] Johannes L Schonberger and Jan-Michael Frahm. Structure-from-motion revisited. In *CVPR (2016)*.
- [39] John Schulman, Filip Wolski, Prafulla Dhariwal, Alec Radford, and Oleg Klimov. Proximal policy optimization algorithms. *arXiv preprint arXiv:1707.06347 (2017)*.
- [40] Gregory C Sharp, Sang W Lee, and David K Wehe. ICP registration using invariant features. *IEEE Transactions on Pattern Analysis and Machine Intelligence (2002)*, 24(1):90–102.
- [41] Jamie Shotton, Ben Glocker, Christopher Zach, Shahram Izadi, Antonio Criminisi, and Andrew Fitzgibbon. Scene coordinate regression forests for camera relocalization in RGB-D images. In *CVPR (2013)*.
- [42] Pascal W Theiler, Jan D Wegner, and Konrad Schindler. Fast registration of laser scans with 4-points congruent sets-what works and what doesn't. *ISPRS annals of the photogrammetry, remote sensing and spatial information sciences (2014)*, 2:149–156.
- [43] Pascal Willy Theiler, Jan Dirk Wegner, and Konrad Schindler. Keypoint-based 4-points congruent sets—automated marker-less registration of laser scans. *ISPRS journal of photogrammetry and remote sensing (2014)*, 96:149–163.
- [44] Ben J Tordoff and David William Murray. Guided-MLESAC: Faster image transform estimation by using matching priors. *IEEE transactions on pattern analysis and machine intelligence (2005)*, 27(10):1523–1535.
- [45] Philip HS Torr and Andrew Zisserman. MLESAC: A new robust estimator with application to estimating image geometry. *Computer vision and image understanding (2000)*, 78(1):138–156.
- [46] Ngoc-Trung Tran, Dang-Khoa Le Tan, Anh-Dzung Doan, Thanh-Toan Do, Tuan-Anh Bui, Mengxuan Tan, and Ngai-Man Cheung. On-device scalable image-based localization via prioritized cascade search and fast one-many ransac. *IEEE Transactions on Image Processing (2020)*, 28(4):1675–1690.
- [47] Lingjing Wang, Xiang Li, and Yi Fang. Unsupervised learning of 3D point set registration. *arXiv preprint arXiv:2006.06200 (2020)*.
- [48] Yue Wang and Justin M Solomon. Deep closest point: Learning representations for point cloud registration. In *ICCV (2019)*.
- [49] Yue Wang and Justin M Solomon. PRNet: Self-supervised learning for partial-to-partial registration. *arXiv preprint arXiv:1910.12240 (2019)*.
- [50] Yue Wang, Yongbin Sun, Ziwei Liu, Sanjay E Sarma, Michael M Bronstein, and Justin M Solomon. Dynamic graph cnn for learning on point clouds. *Acm Transactions On Graphics (2019)*, 38(5):1–12.
- [51] Zhirong Wu, Shuran Song, Aditya Khosla, Fisher Yu, Linguang Zhang, Xiaoou Tang, and Jianxiong Xiao. 3D shapenets: A deep representation for volumetric shapes. In *CVPR (2015)*.
- [52] Yusheng Xu, Richard Boerner, Wei Yao, Ludwig Hoegner, and Uwe Stilla. Pairwise coarse registration of point clouds in urban scenes using voxel-based 4-planes congruent sets. *ISPRS journal of photogrammetry and remote sensing (2019)*, 151:106–123.
- [53] Jiaolong Yang, Hongdong Li, and Yunde Jia. Go-ICP: Solving 3D registration efficiently and globally optimally. In *ICCV (2013)*.
- [54] Lei Yang, Wenxi Liu, Zhiming Cui, Nenglu Chen, and Wenping Wang. Mapping in a cycle: Sinkhorn regularized unsupervised learning for point cloud shapes. In *ECCV (2020)*.
- [55] Zi Jian Yew and Gim Hee Lee. RPM-Net: Robust point matching using learned features. In *CVPR (2020)*.
- [56] Wentao Yuan, Benjamin Eckart, Kihwan Kim, Varun Jampani, Dieter Fox, and Jan Kautz. DeepGMR: Learning latent gaussian mixture models for registration. In *ECCV (2020)*.
- [57] Ji Zhang and Sanjiv Singh. LOAM: Lidar odometry and mapping in real-time. In *RSS (2014)*.
- [58] Qian-Yi Zhou, Jaesik Park, and Vladlen Koltun. Fast global registration. In *ECCV (2016)*.
- [59] Jing Zhu and Yi Fang. Reference grid-assisted network for 3D point signature learning from point clouds. In *WACV (2020)*.